doi:10.1016/S0022-2836(03)00113-X J. Mol. Biol. (2003) 327, 203–214

JMB

Available online at www.sciencedirect.com

SCIENCE DIRECT®

Supramodular structure and synergistic target binding of the N-terminal tandem PDZ domains of PSD-95

Jia-Fu Long[1], Hidehito Tochio[1], Ping Wang[1], Jing-Song Fan[1] Carlo Sala[2], Martin Niethammer[2], Morgan Sheng[2]* and Mingjie Zhang[1]*

[1]*Department of Biochemistry Molecular Neuroscience Center The Hong Kong University of Science and Technology Clear Water Bay Kowloon, Hong Kong People's Republic of China*

[2]*Picower Center for Learning and Memory, Howard Hughes Medical Institute Massachusetts Institute of Technology, Cambridge MA 02139, USA*

**Corresponding author*

PDZ domain proteins play critical roles in binding, clustering and subcellular targeting of membrane receptors and ion channels. PDZ domains in multi-PDZ proteins often are arranged in groups with highly conserved spacing and intervening sequences; however, the functional significance of such tandem arrangements of PDZs is unclear. We have solved the three-dimensional structure of the first two PDZ domains of postsynaptic density protein-95 (PSD-95 PDZ1 and PDZ2), which are closely linked to each other in the PSD-95 family of scaffold proteins. The two PDZs have limited freedom of rotation and their C-terminal peptide-binding grooves are aligned with each other with an orientation preference for binding to pairs of C termini extending in the same direction. Increasing the spacing between PDZ1 and PDZ2 resulted in decreased binding between PDZ12 and its dimeric targets. The same mutation impaired the functional ability of PSD-95 to cluster Kv1.4 potassium channels in heterologous cells. The data presented provide a molecular basis for preferential binding of PSD-95 to multimeric membrane proteins with appropriate C-terminal sequences.

Keywords: PSD-95; PDZ domain; modular structure; receptor clustering; scaffolding protein

Introduction

The PDZ (postsynaptic density-95, disc-large, and zonulin-1) domain is one of the most abundant protein interaction modules in eukaryotic genomes.[1,2] PDZ domain-containing proteins play central roles in organizing signal transduction complexes, clustering membrane receptors, and maintaining cell polarities.[3–6] A typical PDZ domain contains ~90 amino acid residues, and binds specifically to a short peptide at the extreme carboxyl end of target proteins.[7] PDZ domains can bind to internal sequences that fold in a β-hairpin structure.[8–10]

PDZ domains are often arranged in closely linked groups within proteins containing multiple PDZ domains. For example, the PSD-95 (also known as SAP90) family of membrane-associated guanylate kinases contain two N-terminal PDZ repeats (PDZ1 and PDZ2) connected in tandem by a conserved peptide linker of less than five amino acid residues. The conservation of short length and sequence suggests that the PDZ1/2 linker of PSD-95 family proteins is not just "passively" connecting the two PDZ domains. Recent biochemical analysis showed that sequential arrangement of PDZ1 and PDZ2 is important for PSD-95 mediated ion-channel clustering.[11] The PDZ domains of the GRIP/ABP family of AMPA receptor binding proteins show a conserved clustering of the first three (PDZ123), and second three (PDZ456) PDZ domains.[12,13] Effective GluR2/3 binding requires the presence of tandem PDZs (PDZ45).[13–15]

Close linkage of PDZ domains is found in smaller adaptor proteins. The two PDZ domains of mammalian syntenins are separated by a conserved four amino acid linker (DRPF),[16] again suggesting that the linker is not simply acting as a spacer between the two PDZ domains. Both *in vitro* syntenin-syndecan binding and proper membrane localization of syntenin require the paired PDZ domains.[16–18] Emerging evidence suggests that tandemly arranged PDZ repeats possess

Abbreviations used: AMPA, α-amino-3-hydroxy-5-methyl-4-isoxazole; ED_{50}, concentration at 50% effective dissociation; GST, glutathione transferase; NMDA, *N*-methyl-D-aspartate; NOE, nuclear Overhauser enhancement; NOESY, NOE spectroscopy; PSD-95, postsynaptic density-95; Trx, thioredoxin.

E-mail addresses of the corresponding authors: mzhang@ust.hk; msheng@mit.edu

0022-2836/03/$ - see front matter

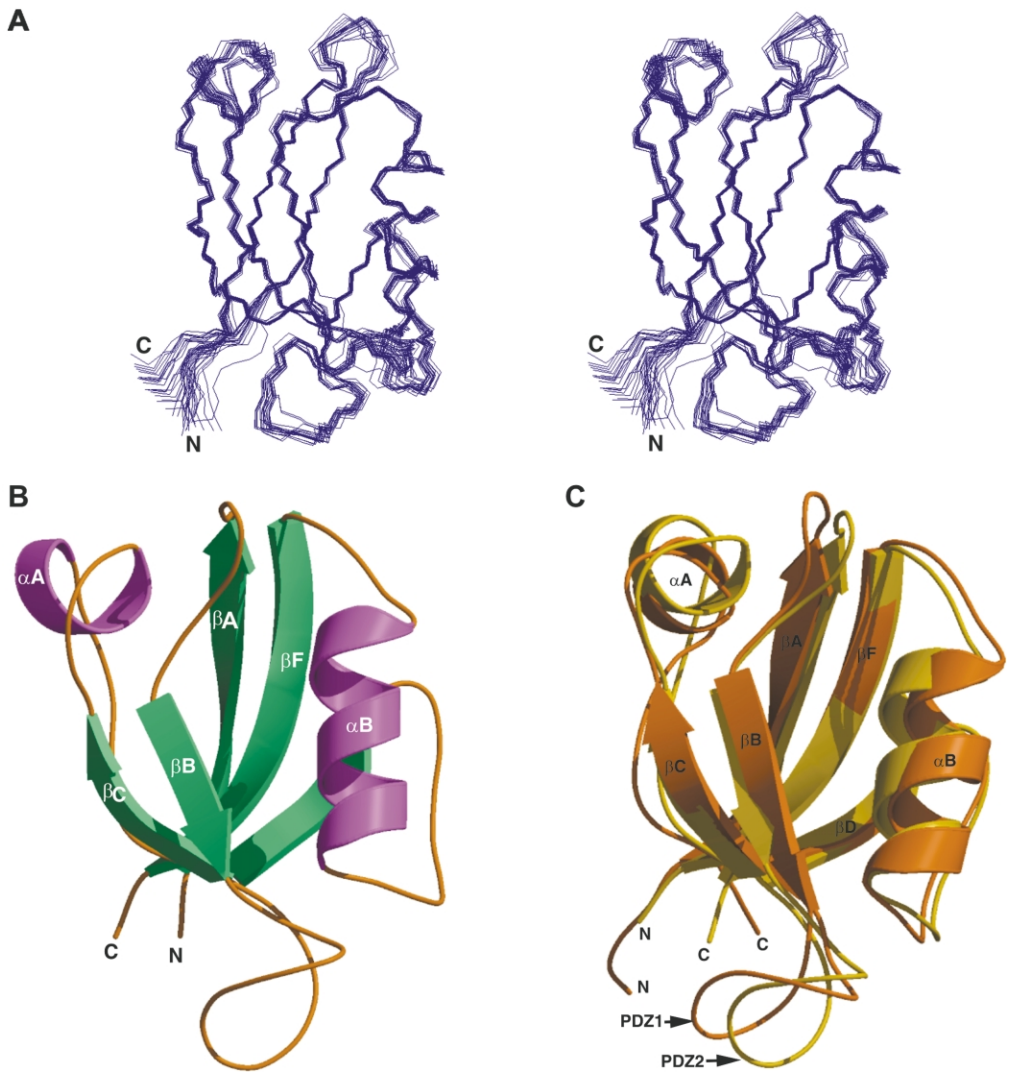

Figure 1. Structure of PSD-95 PDZ1 determined by NMR spectroscopy. (A) Stereoview showing the best-fit superposition of the backbone atoms (N, C^{α}, and C′) of the final 20 structures of PSD-95 PDZ1. The structures are superimposed against the average structure using the residues 64–148. The structural statistics are summarized in Table 1. (B) Ribbon diagram presentation of PSD-95 PDZ1. The secondary structure elements are labelled following the scheme used in the crystal structure of PSD-95 PDZ3.[7] (C) Comparison of the 3D structures of PDZ1 and PDZ2 of PSD-95. The backbone traces (N, C^{α}, and C′) of PDZ1 (gold) and PDZ2 (yellow) are superimposed. The two structures were fit to each other by excluding the GLGF-loop, βB/βC loop and the two termini. The rmsd between the backbones of the two PDZ domains is 1.35 Å.

functional features that differ from the simple sum of the individual PDZ domains. However, there is currently no structural understanding of linked groups of PDZ domains that could provide insights into the special functional properties of tandem PDZs.

We present here the three-dimensional structure of the PDZ12 of PSD-95 linked in tandem. The structure provides a molecular basis for concerted ligand-binding of such PDZ repeats. We further demonstrate that PDZ12 (but not PDZ1 or PDZ2 individually) binds to a dimeric ligand synergistically. A PSD-95 mutant in which PDZ1 and PDZ2 are separated more widely shows decreased synergism in dimeric peptide binding. The same mutant of PSD-95 displayed a poorer clustering of the Kv1.4 potassium channel. The functional implications of PDZ domains arranged in tandem are discussed.

Results

Solution structure of PSD-95 PDZ1

To characterize the structure and dynamics of PDZ12, we first determined the solution structure of PDZ1 using conventional heteronuclear multidimensional NMR spectroscopic techniques. As expected, PDZ1 folds into a classical PDZ-domain like structure in solution (Figure 1(A) and (B); Table 1). The structure of PDZ1 is particularly similar to

Table 1. Structural statistics for the family of 50 structures of PSD-95 PDZ1

Distance restraints	
Intraresidue ($I - j = 0$)	533
Sequential ($\|I - j\| = 1$)	407
Medium-range ($2 \leq \|i - j\| \leq 4$)	262
Long-range ($\|i - j\| \geq 5$)	577
Hydrogen bond	68
Total	1847
Dihedral angle restraints	106
Mean rms deviations from experimental restraints	
Distance (Å)	0.019 ± 0.001
Dihedral angle (deg.)	0.30 ± 0.04
Mean rms deviations from idealized covalent geometry	
Bond (Å)	0.0028 ± 0.0001
Angle (deg.)	0.45 ± 0.01
Improper (deg.)	0.37 ± 0.02
Mean energies (kcal mol^{-1})	
E_{noe}	45.3 ± 3.8
E_{cdih}[a]	0.53 ± 0.11
E_{L-J}	−131.8 ± 11.3
Ramachandran plot[b]	
Residues in the allowed regions (%)	99.1
Atomic rms difference (Å, residues 64–148)[c]	
Backbone heavy-atoms	0.31
All heavy-atom	0.85

None of the structures exhibits distance violations greater than 0.2 Å or dihedral angle violations greater than 2°.

[a] The final values of the square-well NOE and dihedral angle potentials were calculated with force constants of 75 kcal/(mol Å) and 200 kcal/(mol rad^2), respectively.

[b] The program PROCHECK[44] was used to assess the overall quality of the structures.

[c] The precision of the atomic coordinates is defined as the average rms difference between the 50 structures and the mean coordinates of the protein.

that of PDZ2,[19] with a root-mean-square-deviation (rmsd) value of 1.35 Å (Figure 1(C)) in the structured regions. Analogous to PDZ2, PDZ1 contains an ordered, extended βB/βC-loop, which may play a role in target-binding specificity.[19] The structural similarities between the two PDZ domains are reflected by their overlapping target-peptide binding spectra (see Figure 3(A)). The minor differences in target peptide-binding specificities between PDZ1 and PDZ2 of PSD-95 may originate from the divergent amino acid sequences of the βB/βC-loops of the two PDZ domains.

Structural model of PSD-95 PDZ12

It is possible that the short PDZ1-PDZ2 linker may result in direct interaction between these two PDZ domains of PSD-95. To test this possibility, we compared ^{1}H–^{15}N heteronuclear single quantum coherence (HSQC) spectra of PDZ1 and PDZ2 to that of PDZ12. Significant line-broadening as well as chemical-shift changes were observed when we compared the summation spectrum of PDZ1 and PDZ2 to that of PDZ12, indicating that the PDZ1 and PDZ2 can indeed contact each other (Figure 2(A)). Noticeable chemical-shift changes were observed when ^{15}N-labeled PDZ1 was titrated with unlabeled PDZ2 (or ^{15}N-labeled PDZ2 titrated with unlabeled PDZ1), although the scale of chemical shift changes induced by the two separated PDZ domains was much smaller than what was observed in the covalently linked PDZ12 (data not shown). However, such inter-domain interaction between the two PDZ domains is likely to be weak, as we observe significant line-broadening for the amino acid residues that experience domain contact-induced chemical-shift changes.

We then calculated the PDZ12 structure by taking the NMR-derived distance restraints obtained for PDZ1 (Figure 1) and PDZ2[19] using the program CNS.[20] Due to the lack of the inter-domain distance restraints, we opted to use backbone ^{1}H–^{15}N residual dipolar coupling constants (a total of 94 residual dipolar coupling constants measured by dissolving PDZ12 in 20 mg/ml Pf1 phage) as well as chemical shift perturbation data obtained from the titration experiments to derive the relative orientation of the two domains. Figure 2(B) presents the superposition of five calculated structures with lowest energies, and all these structures show limited degrees of orientation preference between the two PDZ domains. This restrained orientation of the two PDZ domains is supported by the backbone dynamics of the protein. The ^{1}H–^{15}N NOE values of the amino acid residues in the PDZ1 and PDZ2 linker region are lower than the well-ordered region, but significantly higher than NOE values observed for completely unordered backbone amides (data not shown). Figure 2(C) shows a representative structure of PDZ12 using a ribbon diagram. The two PDZ domains are arranged side-by-side with their respective βB/βC-loops close to each other. The peptide-binding channels of PDZ1 and PDZ2 are accessible to target proteins. We note that the two target peptide-binding surfaces face in more or less the same direction (Figure 2(C)). The structural features of PDZ12 shown in Figure 2(C) suggest that the two binding channels are capable of binding to dimeric ligands in concert if their C termini point in the same direction; such concerted binding is likely to enhance target-binding affinity. We further note that the two similarly oriented peptide-binding channels of PSD-95 PDZ12 are well suited to bind the carboxyl termini of multimeric receptors and ion channels (such as NMDA receptors, Kv1.4 potassium channels).

PDZ1 and PDZ2 in PSD-95 bind synergistically to bivalent ligands

To test whether the dual peptide-binding channels of PDZ12 function differently from the individual PDZ domains in interacting with bivalent ligands, we used a number of different experimental approaches. First, we used a yeast two-hybrid assay to qualitatively compare target

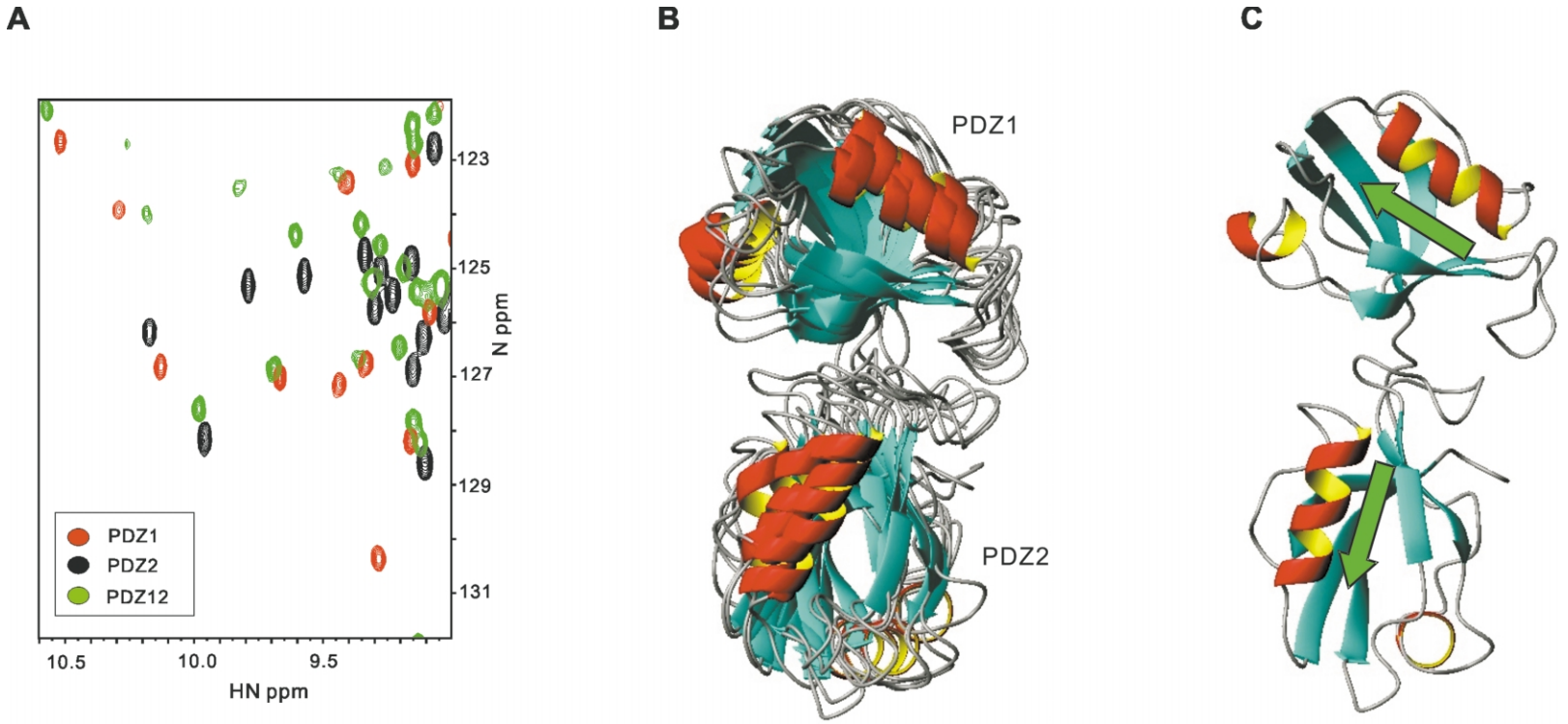

Figure 2. Solution structure of PSD-95 PDZ12. (A) The two PDZ domains in PDZ12 interact with each other. The Figure shows the superposition $^{1}H,^{15}N$ HSQC spectra of ^{15}N-labeled PDZ1 (red), PDZ2 (black), and PDZ12 (green). Both the line-broadening and chemical-shift changes of PDZ12, with respect to the summation spectrum of PDZ1 and PDZ2, indicate that the two PDZ domains in PSD-95 contact each other. (B) Ribbon diagram presentation of five superimposed PDZ12 structures with lowest energies calculated by incorporating residual dipolar coupling constants and chemical-shift perturbation data. None of the structures violated the residual dipolar coupling constants greater than 1 Hz, or distance restraint derived from the chemical-shift perturbation data. The PDZ12 structures were superimposed using all backbone heavy atoms. (C) A representative PDZ12 structure shown as a ribbon diagram. The two peptide-binding channels of PDZ12 are indicated with green arrowheads, and the directions of the arrowheads show the orientations of potential peptide ligands in complex with PDZ12.

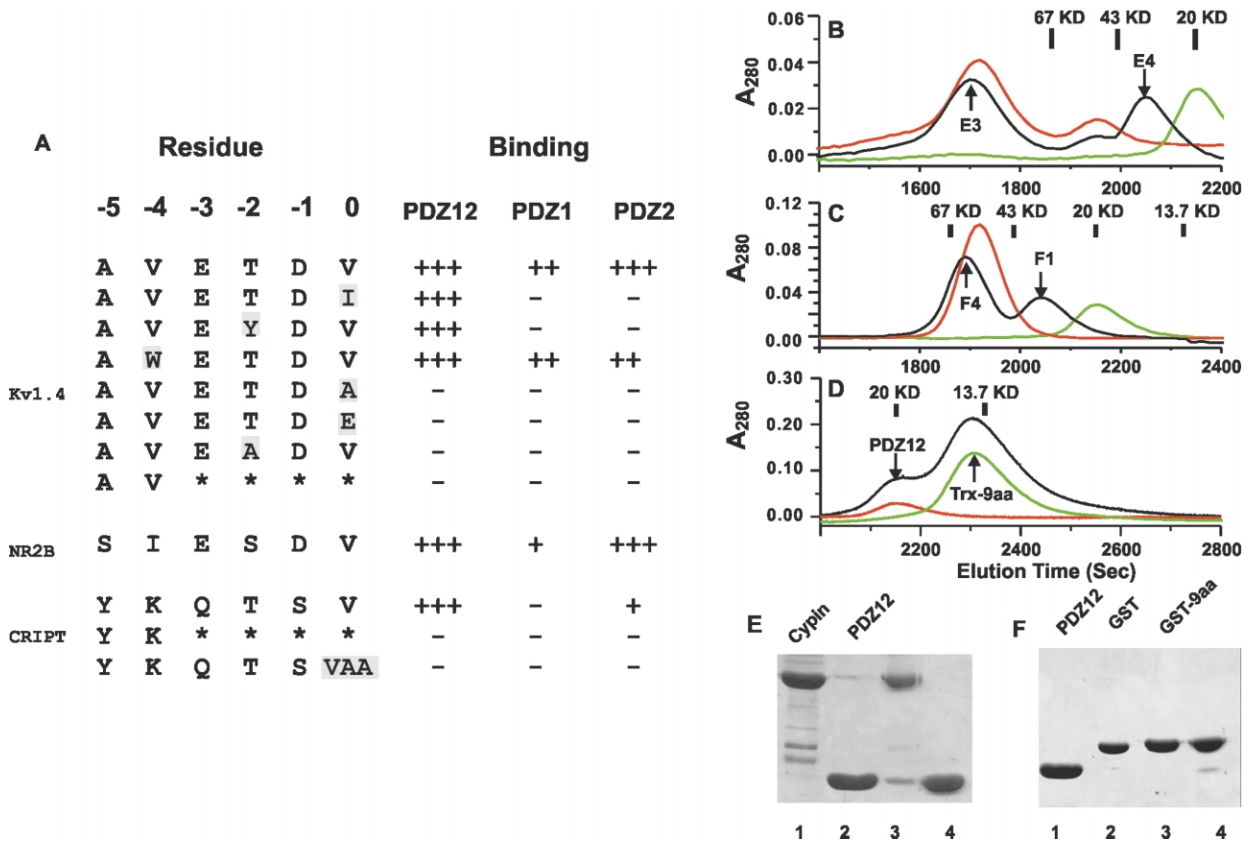

Figure 3. PDZ12 of PSD-95 binds to bivalent ligands synergistically. (A) Yeast two-hybrid assay comparing the interactions of various carboxyl peptides with PDZ1, PDZ2 and PDZ12, respectively. In this assay, the carboxyl peptides were fused to the DNA-binding domain, and the PDZ domains were fused to the activation domain. The interactions between peptides and PDZ domains were categorized into strong (+++), medium (++), weak (+) and no interaction (−). The three peptides used were derived from PSD-95 interacting proteins of the Kv1.4 potassium channel, CRIPT (Cys-rich interactor of PDZ3), and the NR2B subunit of the NMDA receptor. A number of point and trunction mutations (residues deleted are highlighted by *) of the Kv1.4 and the CRIPT peptide were generated to test PDZ domain binding avidity and specificity. (B)–(F) Gel-filtration chromatography analysis of the interaction between PDZ12 and its targets. (B) and (E) A comparison of the elution profile of full-length cypin in the presence (black) and in the absence (red) of a saturating amount of PDZ12. The chromatography profile of free PDZ12 (green) is shown. The protein components of the elution peaks in (B) labeled E3 (lane 3 in (E)) and E4 (lane 4 in (E)) were analyzed by SDS-PAGE. Lanes 1 and 2 in (E) were loaded with pure cypin and PDZ12, respectively. One can clearly observe formation of a cypin/PDZ12 complex based on the data shown in (E) lane 3 (the cypin/PDZ12 complex is in equilbrium with the free cypin and PDZ12, and this explains the difference in band intensity in the lane). (C) and (F) The elution profile of GST fused with the nine C-terminal residues of cypin with (black) and without (red) PDZ12. Again, the elution curve of PDZ12 alone (green) is included. The F4 peak ((F) lane 4) contains a complex formed between GST-9aa and PDZ12, and the F1 peak is the unbound PDZ12 ((F) lane 1). Lanes 2 and 3 are purified GST and GST-9aa as protein markers. (D) A comparison of the elution profiles of the PDZ12 with (black) and without monomeric Trx-9aa (red). Addition of an excess amount of Trx-9aa does not change the elution time of PDZ12, indicating that no stable complex was formed in the gel-filtration column. The chromatography profile of free thioredixin (green) is included. Due to the lack of Trp residues, PDZ12 has lower absorption values at a concentration comparable to the other proteins used in the study. The elution volumes of the protein markers used to calibrate the gel-filtration column are labeled at the top of (B)–(D).

peptide-binding specificity and strength of interaction of PDZ1 and PDZ2 *versus* PDZ12. The carboxyl peptides were fused to the LexA DNA-binding domain ("bait"), and the PDZ domains were fused with the activation domain ("prey") of the two-hybrid system. In this experiment, we took advantage of the fact that the DNA-binding domain forms a dimer, and therefore all peptides were presented to PDZ domains in a "bivalent" manner. For every peptide sequence tested, PDZ12 displayed stronger interaction in the yeast two-hybrid system than either PDZ1 or PDZ2 alone (Figure 3(A)), suggestive of increased avidity of binding. In two cases (last four residues -ETDI, and -EYDV; Figure 3(A) rows 2 and 3), no interaction between peptides and individual PDZ domains could be detected, whereas strong interactions were observed between these two peptides and the tandem PDZ12. In another case, the peptide corresponding to the C-terminal end of CRIPT (-QTSV)[21] binds only weakly to PDZ2, and has no detectable interaction with PDZ1. However,

a strong interaction was detected between this peptide and PDZ12. The overall binding specificity of PDZ12 towards carboxyl-terminal peptides was apparently not compromised when compared to individual PDZ domains. Mutation of the terminal hydrophobic residue Val to Glu or Ala abolished the interaction with PDZ12 as well as PDZ1 and PDZ2. Mutation of the Thr at the −2 position to an amino acid residue without a hydroxyl group on its side-chain disrupted the interaction (Figure 3(A) rows 5–7). As expected, deletion of the last four amino acid residues of the carboxyl peptides, as well as addition of two extra amino acid residues at the C-terminal end of the CRIPT peptide, abolished interactions between these peptides with all of the PDZ domains tested (Figure 3(A)).

Since the yeast two-hybrid data are rather qualitative and indirect, we used gel-filtration chromatography to test whether interactions between PDZ12 and bivalent ligands are stronger than PDZ12 binding to monovalent lignads *in vitro*. In this study, we used a recently identified neuronal protein cypin as PDZ12 target.[22] Analytical gel-filtration experiment showed that full-length cypin exists as a dimer in solution (Figure 3(B), red trace). Mixing PDZ12 with full-length cypin resulted in a complex composed of both cypin and PDZ12 (Figure 3(B) and (E)), and this binary complex has a smaller elution volume (peak labeled E3, black curve) than cypin alone (red curve) (Figure 3(B)). The existence of the cypin/PDZ12 complex in the gel-filtration column is supported by the analysis of the protein composition of the elution peak E3 (Figure 3(B) and (E)). Due to the equilibrium between the cypin/PDZ12 complex and its respective free proteins, the apparent molecular mass of the cypin/PDZ12 is smaller than the theoretical molecular mass of the tight cypin/PDZ12 complex. Such chemical equilibrium accounts for an apparent molecular mass increase of PDZ12 in the gel-filtration profile of cypin/PDZ12 complex (Figure 3(B)). Formation of the complex between PDZ12 and full-length cypin is likely supported by the bivalent feature of the cypin dimer. To test this, we fused the C-terminal nine residue peptide fragment of cypin (which is absolutely required for PSD-95 binding[22]) to either glutathione transferase (GST-9aa) or thioredoxin (Trx-9aa). The crystal structure of GST shows that the protein forms a dimer, and the C-terminal tails of the two subunits are close to each other with near-parallel orientation (hence the cypin peptide in GST-9aa would be presented to PDZ12 with a bivalent structure).[23] In contrast, Trx-9aa exists as a monomer in solution. Consistent with our prediction, a GST-9aa/PDZ12 complex was observed in gel-filtration chromatography (Figure 3(C) and (F)), whereas no obvious PDZ12/Trx-9aa complex was observed even in the presence of an excess amount of Trx-9aa (Figure 3(D)).

Finally, fluorescence titration experiments were employed to obtain a more quantitative picture of PDZ12-enhanced target peptide binding. The yeast two-hybrid experiment showed that replacing Val with a Trp in the-4 position of the Kv1.4 carboxyl peptide does not change its PDZ domain-binding property (Figure 3(A), row 4). Since neither PDZ1 nor PDZ2 contains any Trp residue, the Trp-containing peptide was conveniently used to quantify the interaction between PDZ domains and the peptide. We synthesized a ten residue synthetic peptide with the amino acid sequence CSGSAWETDV. A Cys residue in the N terminus of the peptide was designed to form a disulfide-bond linked homo-dimer of the peptide. The Ser-Gly-Ser tripeptide was inserted to introduce enough space for the dimeric peptide to simultaneously bind to the peptide-binding grooves of PDZ12. Figure 4(A) compares the fluorescence spectra of monomeric (6 μM) and dimeric peptide (3 μM) in the presence of a 9 μM PDZ12. The dimeric peptide displayed a much greater PDZ12 binding-induced fluorescence intensity enhancement than the monomeric peptide (curves 3 and 5), indicating that the dimeric peptide displays a binding property significantly different from that of the monomeric peptide for PDZ12. Figure 4(B) shows fluorescence titration curves of PDZ1, PDZ2 and PDZ12 with the monomeric peptide, and all three binding curves could be fit using a simple Langmuir binding equation with comparable K_d values of 9.7(±0.7), 11.5(±1.3), 7.2(±0.4) μM for the respective PDZ domains. The titration curve of the dimeric peptide with PDZ12 showed that the peptide binds to PDZ12 with 1:1 stoichiometry (Figure 4(C)). Comparison of the titration curve of the monomeric peptide with PDZ12 to that of the dimeric peptide with PDZ12 indicated clearly that the dimeric peptide has a significantly higher binding affinity for PDZ12. Due to the flexibility of the bidentate peptide ligand as well as the partial flexibility of the two domains in the protein, the binding curve of PDZ12 to dimeric peptide could not be fit using a rigid body, 1:1 Langmuir binding equation. To estimate the affinity difference between the monomeric peptide and the dimeric peptide in binding to PDZ12, we therefore performed a binding competition assay using a peptide derived from the carboxyl tail of the NMDA receptor 2 subunit (NR2B) (see also Figure 3(A), row 9). The NR2B peptide (contains the last nine amino acid residues of the receptor with amino acid sequence of KLSSIESDV) effectively competed with the monomeric Kv1.4 peptide for binding to PDZ12 with an ED_{50} of ~5.5 μM. In contrast, the ED_{50} value for competing with the dimeric Kv1.4 peptide is ~100 μM (Figure 4(D)). We conclude that dimeric peptide binds to PDZ12 with ~20-fold higher affinity than the monomeric peptide.

To test whether the short PDZ1-PDZ2 linker is important for the concerted binding of the tandem PDZs to the dimeric peptide, we created a PDZ12 mutant in which a flexible stretch of nine amino acid residues (Ser-Gly-Gly-Ser-Gly-Gly-Ser-Gly-Gly) is inserted in the PDZ1-2 linker region

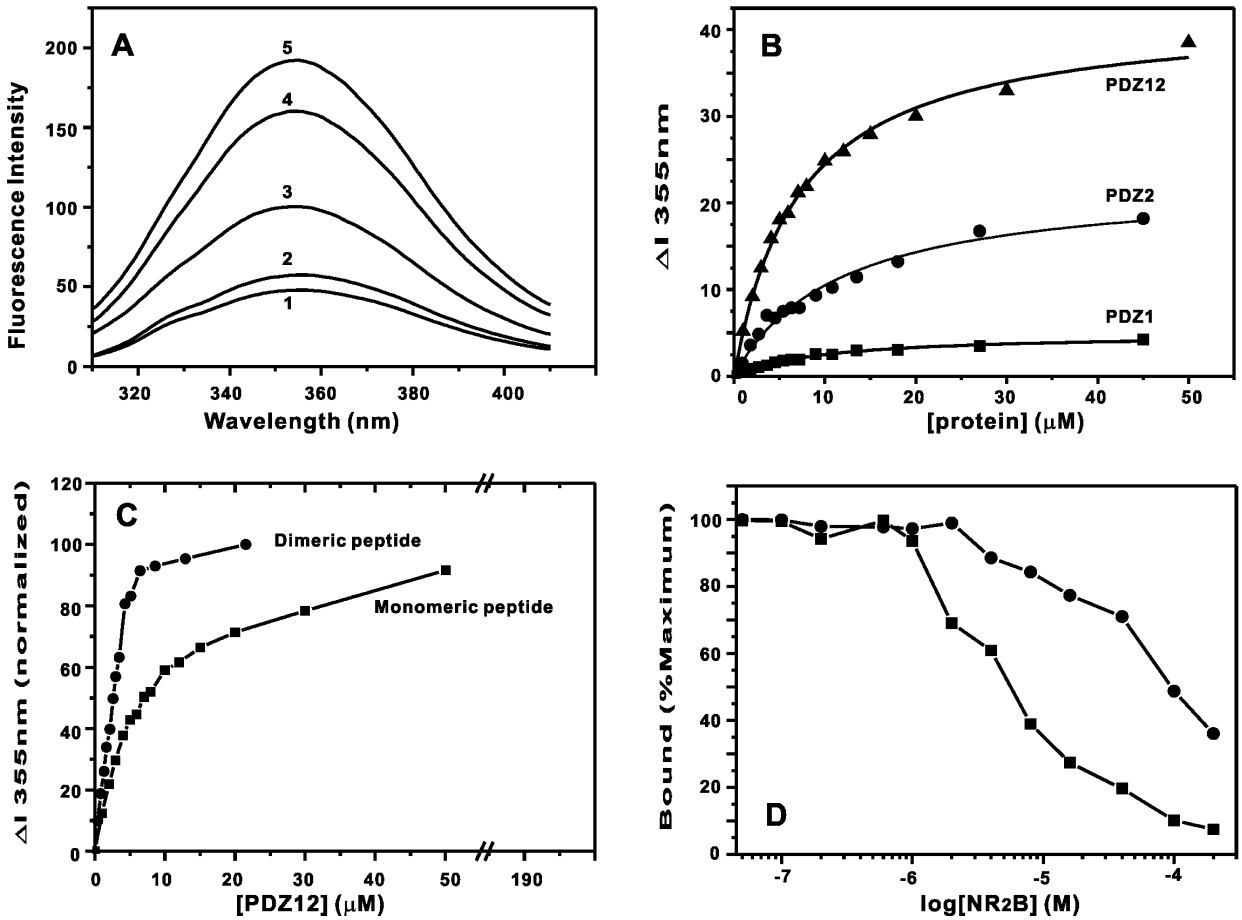

Figure 4. Fluorescence spectroscopic studies of interactions of PDZ12 with monovalent and bivalent peptides. (A) Fluorescence spectra of monomeric and dimeric peptides in complex with PDZ12. Curves 1 and 3 are the spectra of free and PDZ12-saturated forms of the monomeric Kv1.4 peptide, respectively. Curves 2 and 5 represent the spectra of free and PDZ12-saturated dimeric Kv1.4 peptide, respectively. Curve 4 represents the fluorescence spectrum of the Kv1.4 peptide dimer with saturating concentrations of PDZ12Ins mutant. (B) Fluorescence titration curves of monomeric Kv1.4 peptide binding to PDZ1 (■), PDZ2 (●), and PDZ12 (▲). The concentration of the monomeric peptide used in this study is 9 μM for PDZ1 and PDZ2 titration, 18 μM for PDZ12 titration. The continuous curves represent fitting of the experimental data using a simple A + B → AB 1:1 Langmuir binding model. (C) Fluorescence titration curves comparing the binding of the monomeric peptide (■) and the dimeric peptide (●) to PDZ12. To facilitate comparison, the fluorescence intensity is normalized. (D) Competion of the NR2B peptide with the monomeric peptide (■) and the dimeric peptide (●) for binding to PDZ12. In this assay, the Kv 1.4 peptide was pre-incubated with PDZ12 (9 μM monomeric peptide with 9 μM PDZ12, and 4.5 μM dimeric peptide with the same concentration of PDZ12). The *Y*-axis is the percentage of fluorescence intensity decrease with each increment of NR2B concentration.

(referred as PDZ12Ins). PDZ12Ins displayed a decreased dimeric peptide binding-induced fluorescence intensity change compared with wild-type PDZ12 (Figure 4(A), curve 4), indicating that increased separation of PDZ1 and PDZ2 reduced the binding affinity for the dimeric peptide ligand.

If the relative separation and orientation of the two peptide-binding channels of PDZ12 is functionally important for target interaction, insertion of extra sequence into the PDZ1 and PDZ2 linker might be predicted to alter the target-binding properties of PSD-95. One well-characterized activity of PSD-95, which is dependent on PDZ/carboxyl terminal peptide interaction, is the clustering of ion channels and receptors (e.g. Kv1.4 and NMDA receptors) in heterologous cells.[24,25] We compared the Kv1.4 potassium channel clustering activities of wild-type and insertion mutant of PSD-95 in COS cells. It was shown earlier that PDZ12 plus the entire N-terminal segment of PSD-95 (N-PDZ12) is necessary and sufficient for Kv1.4 clustering (Figure 5(A)).[26,27] Although the insertion mutant of N-PDZ12 (N-PDZ12Ins) can still cluster Kv1.4, the resulting Kv1.4 clusters (average area 1.0(± 0.8) μm^2) were significantly smaller than those induced by the wild-type N-PDZ12 (average area 3.1(± 1.1) μm^2) (Figure 5(A) and (B)). The data further suggest that the shortness of the linker between PDZ1 and PDZ2 is functionally important for the ability of PSD-95 to form large clusters with its membrane protein targets. In parallel experiments, a linker deletion mutant of PDZ12 that shortened the linker between PDZ1 and PDZ2 to two amino acid

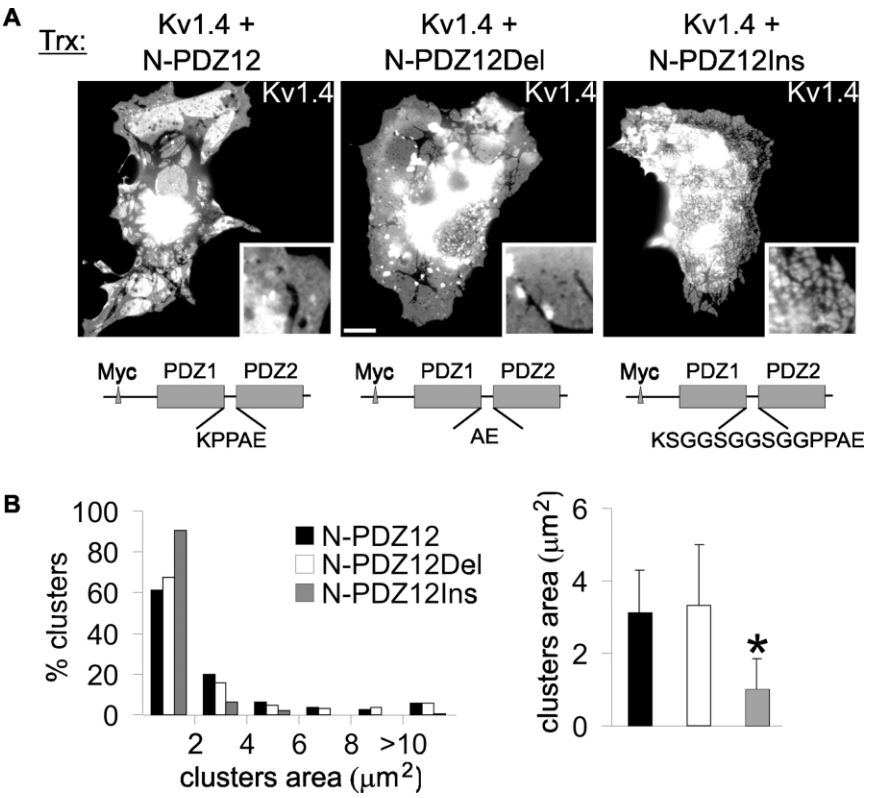

Figure 5. Functional role of conformation-restrained tandem PDZ repeats in PSD-95. (A) Extending the PDZ12 linker by introducing flexible amino acid residues reduces the size of the Kv1.4 channel clusters mediated by N-PDZ12. Myc-tagged constructs N-PDZ1-2 wild-type (N-PDZ12), the deletion mutant of N-PDZ12 (N-PDZ12Del) and the insertion mutant of N-PDZ12 (N-PDZ1-2Ins) were co-transfected in COS7 cells with potassium channel subunit Kv1.4. Cells cotransfected with different constructs, as indicated, were fixed two days after transfection and stained with Kv1.4 antibodies to visualize the potassium channel clusters. The schematics of the deletions and insertion mutations used in this study are shown. Insets show higher-magnification views of Kv1.4 clusters. (B) Frequency distribution (left) and mean values (right) of Kv1.4 cluster areas mediated by N-PDZ12, N-PDZ12(Del) and N-PDZ12(Ins), measured from at least ten cells for each construct. The scale bars represent 5 μm or 15 μm for the insets. An asterisk (*) indicates significance at $p < 0.01$ in an unpaired, two-tailed Student's *t*-test.

residues was created. An *in vitro* peptide-binding experiment did not reveal a difference between the deletion mutant and wild-type PDZ12 (data not shown). The deletion mutation had no significant effect on the size of PSD-95-Kv1.4 clusters (average area 3.3(±1.6) μm^2).

Discussion

This study is the first to characterize the three-dimensional structure of a tandem (supramodular) array of PDZ domains. The first two PDZ domains of PSD-95 have been studied extensively in terms of their interaction with membrane receptors/channels, such as the multimeric NMDA receptor and Shaker-family potassium channels. The NMR analysis reveals that PDZ1 and PDZ2 have a limited degree of rotation relative to each other and that their peptide-binding surfaces face in more or less the same direction. We propose that this supramodular organization is specialized to facilitate interaction of the PDZ12 pair to multimeric membrane proteins, as typified by receptors/ion channels. The synergistic binding of the tandem PDZ12 of PSD-95 to its multimeric membrane targets is supported by the second law of thermodynamics. Realization of such thermodynamic principle in PSD-95 PDZ12 has helped us to explain a number of biological observations in the literature. The study reminds us that one might need to think beyond individual protein domains in experimental design due to the supramodular nature of proteins.

The synergistic effect of the tandem PDZ domains in PSD-95 (and possibly other multi-PDZ proteins) in target binding hints at the functional specialization of supramodular PDZ arrays. One potential significance of tandem PDZ repeats is to bias the binding of PSD-95 toward dimeric/multimeric targets even in the presence of monomeric targets (Figure 6). For example, PDZ12 in a given PSD-95 would tend to bind to the two NR2 tails in a tetrameric NMDA receptor channel.[28] However, such an interaction does not preclude other PSD-95 binding proteins from being physically close to NMDA receptors, as PSD-95 is probably clustered in excess underneath the membrane *via* its N-terminal palmitoyl group. In this context, we note that monomeric interfering peptides conveyed into cells by the Antennapedia method are effective at disrupting PDZ3-mediated interactions of PSD-95 with CRIPT, but ineffective at disrupting PDZ12-mediated interactions with NMDA receptors and Kv1.4 (C.S. & M.S., unpublished observations).[29] Under certain biological conditions, the tandem PDZ domains of PSD-95 should facilitate dimerization of membrane receptors due to entropic advantages contributed by the restrained conformational flexibilities of the

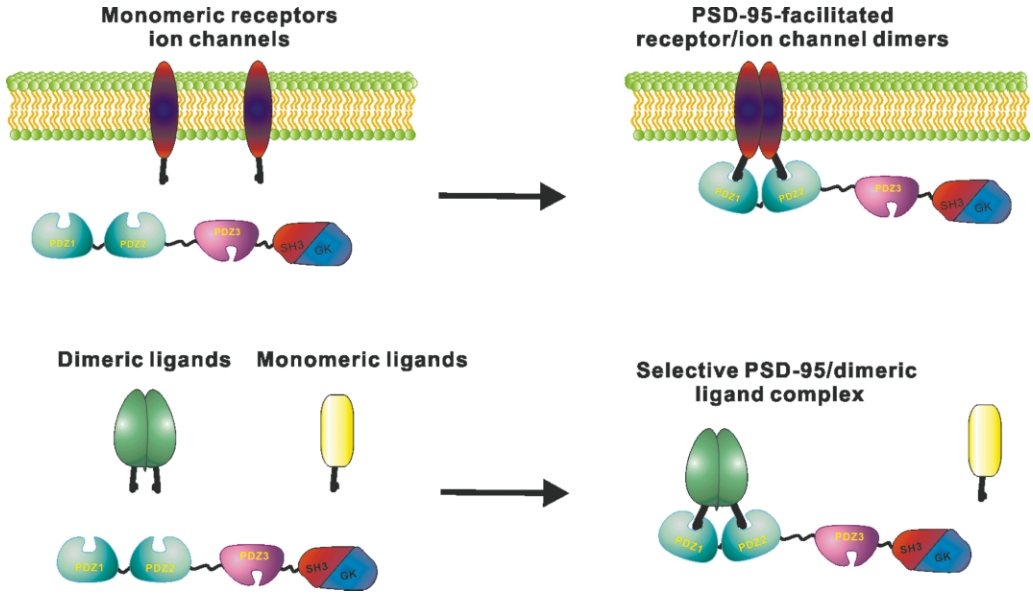

Figure 6. A diagram showing models of possible functions of tandem PDZ12 in PSD-95 in target binding. In the first case, the two conformation-restrained PDZ domains of PSD-95 may serve to promote dimerization of receptors and ion-channels from two monomers. In this case, PDZ12 of PSD-95 may function to stabilize receptor dimer by cross-linking their carboxyl termini. Since PDZ12 of PSD-95 displays a higher binding affinity toward dimeric ligands, the dimeric PSD-95 ligands such as cypin may have a higher priority to interact with PSD-95 even with the presence of monomeric ligands. Under this scenario, the high abundance of cypin may function as a PSD-95 "buffering" protein to regulate its availability to other PSD-95 ligands.

tandem PDZ repeat (Figure 6). It is possible that PSD-95-enhanced activation of ErbB4 receptor tyrosine kinase by neuregulin is mediated by the stabilization of the receptor dimer *via* binding to the PDZ12 of PSD-95.[30,31]

Tandemly arranged protein interaction modules are observed in non-PDZ proteins. In several cases, tandemly arranged protein interaction modules display target-binding properties that are distinct from their respective individual domains. For example, the crystal structure of the tandem SH2 domains of the ZAP-70 non-receptor tyrosine kinase showed that tandemly arranged SH2 domains allow the protein to interact with bidentate phosphotyrosine peptide with exquisite specificity.[32] The double bromodomains in $TAF_{II}250$ lie side-by-side, resulting in a structure ideally suited to interact with bivalent peptide ligands with diacetylated lysine residues.[33] One can envisage that such tandemly arranged protein–protein interaction modules are not just a simple attachment of beads on a string, but often represent functional "supramodules" spatially organized for coordinated binding to specific targets.

Materials and Methods

Cloning, expression, and purification of PSD-95 PDZ1, PDZ2, and PDZ12

PDZ1 (residues 61–151), PDZ2 (residues 155–249) and PDZ12 (residues 61–249) were PCR-amplified from full-length rat PSD-95 gene using appropriate primers, and inserted into the *Xho* I and *Bam* HI sites of the plasmid pET14b (Novagen), respectively. Expression and purification of the recombinant PDZ domains from BL21(DE3) *Escherichia coli* host cells followed the method that we described earlier for PDZ2.[19] Various mutants of PSD-95 PDZ domains used in this study were generated by standard PCR techniques. The mutant proteins were purified using the method that was used for purifying wild-type proteins. Uniformly ^{15}N and $^{15}N/^{13}C$-labeled PDZ domains were prepared by growing the bacteria in M9 minimal medium using $^{15}NH_4Cl$ (1 g/l) as the sole nitrogen source, or $^{15}NH_4Cl$ (1 g/l) and [$^{13}C_6$]glucose (1 g/l) as the sole nitrogen and carbon source, respectively.

Preparation of PDZ-binding peptides

A nine residue synthetic peptide (QVVPFSSSV) corresponding to the last nine residues of rat cypin, a nine residue NR2B peptide (KLSSIESDV) and a ten residue peptide (CSGSAWETDV) derived from the C terminus of the Kv1.4 potassium channel were synthesized commercially (Research Genetics, Huntsville). The peptides were purified by reverse-phase HPLC. To prepare disufide bond-mediated Kv1.4 peptide dimer, the peptide was dissolved in 50 mM Tris–HCl buffer (pH 8.0), and incubated at room temperature for seven days. The dimeric peptide was separated from the unreacted monomeric peptide using reverse-phase HPLC.

Clustering assay of the Kv1.4 potassium channel

The wild-type PSD-95 PDZ12 (GW1-N-PDZ12, residues 1–247 with a Myc-tag inserted between residues 9 and 10 of PSD-95, N-PDZ12) has been described.[34] Insertion (inserting triple Ser-Gly-Gly repeats between Lys and Pro in the PDZ12 linker, and dubbed as

N-PDZ12In′) and deletion (three amino acid residues, KPP, were deleted in the linker and designated as N-PDZ12Del) mutants of GW1-N-PDZ12 were generated by PCR. GW1 expression constructs of the wild-type N-PDZ12 has been described.[26]

Co-transfection of COS7 cells with N-PDZ12 (or its insertion/deletion mutants) and Kv1.4 followed the method described earlier.[26] The cells were fixed by formaldehyde two days after transfection and stained with Kv1.4 antibody, followed by Cy3 and fluorescein isothiocyanate-conjugated secondary antibody (Jackson ImmunoResearch). The Kv1.4 cluster area was measured using MetaMorph image analysis software (Universal Imaging Corp).

Gel-filtration chromatography

Analytical gel-filtration chromatography was carried out on a Bio-Rad Biologic FPLC system using a Superose 12 10/30 column (Amersham Pharmacia Biotech). Protein samples were dissolved in 50 mM Tris–HCl buffer (pH 7.5) in the presence of freshly dissolved dithiothreitol (1 mM). The column was calibrated with the low molecular mass column calibration kit from Amersham Pharmacia Biotech.

Fluorescence experiments

Fluorescence titrations of peptide ligands with PSD-95 PDZ domains were carried out on a Perkin–Elmer LS50B fluorometer. Excitation and emission bandwiths were set at 10 nm and 5 nm, respectively. An excitation wavelength of 295 nm was selected for optimal observation of the intrinsic fluorescence contributed by the Trp residue(s) of the peptide ligands. The data were analyzed using the Microcal Origin curve fitting software.

NMR experiments

NMR spectra were acquired at 30 °C on Varian Inova 500 and 750 MHz spectrometers. Sequential backbone and non-aromatic, non-exchangeable side-chain resonance assignments of the protein were obtained by standard heteronuclear correlation experiments including HNCO, HNCA, HN(CO)CA, HNCACB, CBCA(CO)NH, and HCCH total correlated spectroscopy (TOCSY) experiments, and confirmed by a 3D ^{15}N-separated NOESY experiment.[35,36] The side-chains of aromatics were assigned by ^{1}H 2D TOCSY/nuclear Overhauser enhancement spectroscopy (NOESY) experiments of an unlabeled protein sample in $^{2}H_2O$.[37] The residual dipolar coupling constants of PSD-95 PDZ12 were obtained by recording the in-phase/anti-phase (IPAP) ^{1}H–^{15}N heteronuclear single quantum correlated (HSQC) spectra of the protein in the absence and in the presence of 20% Pf1 phage.[38]

Structural calculations

Approximate interproton distance restraints were derived from NOESY spectra (a ^{1}H 2D homonuclear NOESY, a ^{15}N-separated-NOESY and a ^{13}C-separated NOESY). NOEs were grouped into three distance ranges 1.8–2.7 Å (1.8–2.9 Å for NOEs involving NH protons), 1.8–3.3 Å (1.8–3.5 Å for NOEs involving NH protons), and 1.8–5.0 Å, corresponding to strong, medium, and weak NOEs. Hydrogen bonding restraints (two per hydrogen bond where $r_{NH-O} = 1.8–2.2$ Å and $r_{N-O} =$ 2.2–3.3 Å) were generated from the standard secondary structure of the protein based on the NOE patterns, and backbone secondary chemical-shifts. Backbone dihedral angle restraints (ϕ and ψ angles) were derived from $^{3}J_{HN\alpha}$ coupling constants measured using an HNHA experiment and backbone chemical-shift analysis program TALOS.[39] Structures were calculated using the program CNS.[20] In the calculation of the PDZ12 structural model, residual dipolar coupling constant restraints were incorporated into the structural calculation as described.[40] The chemical-shift perturbations observed in the ^{1}H–^{15}N HSQC titration experiments were used as distance restraints of the two domains. Perturbed amino acid residues were classified into two groups on the basis of whether they belong to PDZ1 or PDZ2. A loose distance restraint (15 Å) between a pair of H^{α} atoms from these two groups was used in the calculation. The Figures were generated using MOLMOL,[41] MOLSCRIPT,[42] and Raster3D.[43]

Protein Data Bank accession numbers

The coordinates of the PSD-95 PDZ1 have been deposited in the Protein Data Bank (PDB) under the accession number of 1IU0 and 1IU2 for the energy minimized structure and the final 50 structures with lowest energies, respectively.

Acknowledgements

We thank Dr Henry Mok for his help at the initial stage of the project. This work was supported, in part, by grants from the Research Grant Council of Hong Kong to M.Z. (HKUST6198/99M, 6207/00M, 6097/01M, and 6125/02M) and by a grant from the Human Frontiers Science Program Organization to M.Z. (RG0068/00M). M.S. is an Associate Investigator of the Howard Hughes Medical Institute.

References

1. Venter, J. C., Adams, M. D., Myers, E. W., Li, P. W., Mural, R. J., Sutton, G. G. *et al.* (2001). The sequence of the human genome. *Science*, **291**, 1304–1351.
2. International Human Genome Sequence Consortium. (2001). Initial sequencing and analysis of the human genome. *Nature*, **409**, 860–921.
3. Craven, S. E. & Bredt, D. S. (1998). PDZ proteins organize synaptic signaling pathways. *Cell*, **93**, 495–498.
4. Fanning, A. S. & Anderson, J. M. (1999). PDZ domains: fundamental building blocks in the organization of protein complexes at the plasma membrane. *J. Clin. Invest.* **103**, 767–772.
5. Garner, C. C., Nash, J. & Huganir, R. L. (2000). PDZ domains in synapse assembly and signalling. *Trends Cell. Biol.* **10**, 274–280.
6. Sheng, M. & Sala, C. (2001). PDZ domains and the organization of supramolecular complexes. *Annu. Rev. Neurosci.* **24**, 1–29.
7. Doyle, D. A., Lee, A., Lewis, J., Kim, E., Sheng, M. & MacKinnon, R. (1996). Crystal structures of a complexed and peptide-free membrane protein-binding

domain: molecular basis of peptide recognition by PDZ. *Cell*, **85**, 1067–1076.
8. Hillier, B. J., Christopherson, K. S., Prehoda, K. E., Bredt, D. S. & Lim, W. A. (1999). Unexpected modes of PDZ domain scaffolding revealed by structure of nNOS–syntrophin complex. *Science*, **284**, 812–815.
9. Tochio, H., Zhang, Q., Mandal, P., Li, M. & Zhang, M. (1999). Solution structure of the extended neuronal nitric oxide synthase PDZ domain complexed with an associated peptide. *Nature Struct. Biol.* **6**, 417–421.
10. Tochio, H., Mok, Y. K., Zhang, Q., Kan, H. M., Bredt, D. S. & Zhang, M. (2000). Formation of nNOS/PSD-95 PDZ dimer requires a preformed beta-finger structure from the nNOS PDZ domain. *J. Mol. Biol.* **303**, 359–370.
11. Imamura, F., Maeda, S., Doi, T. & Fujiyoshi, Y. (2002). Ligand binding of the second PDZ domain regulates clustering of PSD-95 with the Kv1.4 potassium channel. *J. Biol. Chem.* **277**, 3640–3646.
12. Dong, H., O'Brien, R. J., Fung, E. T., Lanahan, A. A., Worley, P. F. & Huganir, R. L. (1997). GRIP: a synaptic PDZ domain-containing protein that interacts with AMPA receptors. *Nature*, **386**, 279–284.
13. Srivastava, S., Osten, P., Vilim, F. S., Khatri, L., Inman, G., States, B. *et al.* (1998). Novel anchorage of GluR2/3 to the postsynaptic density by the AMPA receptor-binding protein ABP. *Neuron*, **21**, 581–591.
14. Dong, H., Zhang, P., Song, I., Petralia, R. S., Liao, D. & Huganir, R. L. (1999). Characterization of the glutamate receptor-interacting proteins GRIP1 and GRIP2. *J. Neurosci.* **19**, 6930–6941.
15. Zhang, Q., Fan, J.-S. & Zhang, M. (2001). Interdomain chaperoning between PSD-95 Dlg, and Zo-1 (PDZ) domains of glutamate receptor-interacting proteins. *J. Biol. Chem.* **276**, 43216–43220.
16. Zimmermann, P., Tomatis, D., Rosas, M., Grootjans, J., Leenaerts, I., Degeest, G. *et al.* (2001). Characterization of syntenin, a syndecan-binding PDZ protein, as a component of cell adhesion sites and microfilaments. *Mol. Biol. Cell.* **12**, 339–350.
17. Grootjans, J. J., Reekmans, G., Ceulemans, H. & David, G. (2000). Syntenin-syndecan binding requires syndecan-synteny and the co-operation of both PDZ domains of syntenin. *J. Biol. Chem.* **275**, 19933–19941.
18. Zimmermann, P., Meerschaert, K., Reekmans, G., Leenaerts, I., Small, J. V., Vandekerckhove, J. *et al.* (2002). PIP(2)-PDZ domain binding controls the association of syntenin with the plasma membrane. *Mol. Cell.* **9**, 1215–1225.
19. Tochio, H., Hung, F., Li, M., Bredt, D. S. & Zhang, M. (2000). Solution structure and backbone dynamics of the second PDZ domain of postsynaptic density-95. *J. Mol. Biol.* **295**, 225–237.
20. Brunger, A. T., Adams, P. D., Clore, G. M., DeLano, W. L., Gros, P., Grosse-Kunstleve, R. W. *et al.* (1998). Crystallography and NMR system (CNS): a new software suite for macromolecular structure determination. *Acta Crystallog. sect. D*, **54**, 905–921.
21. Niethammer, M., Valtschanoff, J. G., Kapoor, T. M., Allison, D. W., Weinberg, T. M., Craig, A. M. & Sheng, M. (1998). CRIPT, a novel postsynaptic protein that binds to the third PDZ domain of PSD-95/SAP90. *Neuron*, **20**, 693–707.
22. Firestein, B. L., Brenman, J. E., Aoki, C., Sanchez-Perez, A. M., El-Husseini, A. E. & Bredt, D. S. (1999). Cypin: a cytosolic regulator of PSD-95 postsynaptic targeting. *Neuron*, **24**, 659–672.
23. McTigue, M. A., Williams, D. R. & Tainer, J. A. (1995). Crystal structures of a schistosomal drug and vaccine target: glutathione *S*-transferase from *Schistosoma japonica* and its complex with the leading antischistosomal drug praziquantel. *J. Mol. Biol.* **246**, 21–27.
24. Kim, E., Niethammer, M., Rothschild, A., Jan, Y. N. & Sheng, M. (1995). Clustering of Shaker-type K^+ channels by interaction with a family of membrane-associated guanylate kinases. *Nature*, **378**, 85–88.
25. Kim, E., Cho, K. O., Rothschild, A. & Sheng, M. (1996). Heteromultimerization and NMDA receptor-clustering activity of Chapsyn-110, a member of the PSD-95 family of proteins. *Neuron*, **17**, 103–113.
26. Hsueh, Y. P. & Sheng, M. (1999). Requirement of N-terminal cysteines of PSD-95 for PSD-95 multimerization and ternary complex formation, but not for binding to potassium channel Kv1.4. *J. Biol. Chem.* **274**, 532–536.
27. Craven, S. E., El-Husseini, A. E. & Bredt, D. S. (1999). Synaptic targeting of the postsynaptic density protein PSD-95 mediated by lipid and protein motifs. *Neuron*, **22**, 497–509.
28. Behe, P., Stern, P., Wyllie, D. J., Nassar, M., Schoepfer, R. & Colquhoun, D. (1995). Determination of NMDA NR1 subunit copy number in recombinant NMDA receptors. *Proc. Roy. Soc. London*, **262**, 205–213.
29. Passafaro, M., Sala, C., Niethammer, M. & Sheng, M. (1999). Microtubule binding by CRIPT and its potential role in the synaptic clustering of PSD-95. *Nature Neurosci.* **2**, 1063–1069.
30. Garcia, R. A., Vasudevan, K. & Buonanno, A. (2000). The neuregulin receptor ErbB-4 interacts with PDZ-containing proteins at neuronal synapses. *Proc. Natl Acad. Sci. USA*, **97**, 3596–3601.
31. Huang, Y. Z., Won, S., Ali, D. W., Wang, Q., Tanowitz, M., Du, Q. S. *et al.* (2000). Regulation of neuregulin signaling by PSD-95 interacting with ErbB4 at CNS synapses. *Neuron*, **26**, 443–455.
32. Hatada, M. H., Lu, X., Laird, E. R., Green, J., Morgenstern, J. P., Lou, M. *et al.* (1995). Molecular basis for interaction of the protein tyrosine kinase ZAP-70 with the T-cell receptor. *Nature*, **377**, 32–38.
33. Jacobson, R. H., Ladurner, A. G., King, D. S. & Tjian, R. (2000). Structure and function of a human TAFII250 double bromodomain module. *Science*, **288**, 1422–1425.
34. Hsueh, Y. P., Kim, E. & Sheng, M. (1997). Disulfide-linked head-to-head multimerization in the mechanism of ion channel clustering by PSD-95. *Neuron*, **18**, 803–814.
35. Kay, L. E. & Gardner, K. H. (1997). NMR solution spectroscopy beyond 25 kDa. *Curr. Opin. Struct. Biol.* **7**, 722–731.
36. Clore, G. M. & Gronenborn, A. M. (1998). Determining the structures of large proteins and protein complexes by NMR. *Trends Biotechnol.* **16**, 22–34.
37. Wüthrich, K. (1986). *NMR of Proteins and Nucleic Acids*, Wiley, New York.
38. Ottiger, M., Delaglio, F. & Bax, A. (1998). Measurement of *J* and dipolar couplings from simplified two-dimensional NMR spectra. *J. Magn. Reson.* **131**, 373–378.
39. Cornilescu, G., Delaglio, F. & Bax, A. (1999). Protein backbone angle restraints from searching a database for chemical shift and sequence homology. *J. Biomol. NMR*, **13**, 289–302.
40. Blomberg, N., Baraldi, E., Sattler, M., Saraste, M. & Nilges, M. (2000). Structure of a PH domain from

the *C. elegans* muscle protein UNC-89 suggests a novel function. *Struct. Fold. Des.* **8**, 1079–1087.
41. Koradi, R., Billeter, M. & Wuthrich, K. (1996). MOLMOL: a program for display and analysis of macromolecular structures. *J. Mol. Graph.* **14**, 51–55.
42. Kraulis, P. J. (1991). MOLSCRIPT: a program to produce both detailed and schematic plots of protein structures. *J. Appl. Crystallog.* **24**, 946–950.
43. Merritt, E. & Murphy, M. (1994). Raster3D version 2.0: a program for photorealistic molecular graphics. *Acta Crystallog. sect. D*, **50**, 869–873.
44. Laskowski, R. A., Rullmannn, J. A., MacArthur, M. W., Kaptein, R. & Thornton, J. M. (1996). AQUA and PROCHECK-NMR: programs for checking the quality of protein structures solved by NMR. *J. Biomol. NMR.* **8**, 477–486.

Edited by M. F. Summers

(Received 19 November 2002; received in revised form 13 January 2003; accepted 14 January 2003)